ADVANCED MATERIALS
www.advmat.de

Color-Tunable Organic Light-Emitting Diodes with Single Pt (O^N^C^N)-Dibenzofuran Emitter Exhibiting High External Quantum Efficiency of ≈30% and Superior Operational Lifetime

Mao Mao, Huiyang Li, Kar-Wai Lo, Dongdong Zhang, Lian Duan, Shuo Xu, Qingyun Wan, Kaixin Tan, Pengcheng An, Gang Cheng,* and Chi-Ming Che**

Color-tunable organic light-emitting diodes (CT-OLEDs) have a large color-tuning range, high efficiency and operational stability at practical luminance, making them ideal for human-machine interactive terminals of wearable biomedical devices. However, the device operational lifetime of CT-OLEDs is currently far from reaching practical requirements. To address this problem, a tetradentate Pt(II) complex named tetra-Pt-dbf, which can emit efficiently in both monomer and aggregation states, is designed. This emitter has high T_d of 508 °C and large intermolecular bonding energy of -52.0 kcal mol^{-1}, which improve its thermal/chemical stability. This unique single-emitter CT-OLED essentially avoids the "color-aging issue" and achieves a large color-tuning span (red to yellowish green) and a high external quantum efficiency (EQE) of ≈30% at 1000 cd m^{-2} as well as an EQE of above 25% at 10000 cd m^{-2}. A superior LT_{90} operational lifetime of 520,536 h at a functional luminance of 100 cd m^{-2}, which is over 20 times longer than the state-of-the-art CT-OLEDs, is estimated. To demonstrate the potential application of such OLEDs in wearable biomedical devices, a simple electromyography (EMG)-visualization system is fabricated using the CT-OLEDs.

1. Introduction

In recent years, organic light-emitting diodes (OLEDs) have made significant progress in operational stability, making them increasingly mature in the field of commercial display panels.[1–4] Due to their ultra-thin thickness, energy-saving, and mechanical flexibility, they are now expected to play an important role in other fields that demand monochromatic and tunable chromaticity,[5–10] such as smart lighting and point-of-care wearable biomedical sensors.[5,6,8,11,12] OLED types with continuously tunable color and fast response rate, called color-tunable OLEDs (CT-OLEDs), have been invented and attracted widespread interest in the past two decades.[5,11–16] Most of the work focuses on exploiting different colors of two independent sub-OLEDs and applying alternating current or varying voltages to adjust the emission ratio of each sub-OLED.[13,17]

M. Mao, H. Li, K.-W. Lo, S. Xu, Q. Wan, K. Tan, G. Cheng, C.-M. Che
State Key Laboratory of Synthetic Chemistry
Department of Chemistry
The University of Hong Kong
Pokfulam Road, Hong Kong SAR P. R. China
E-mail: ggcheng@hku.hk; cmche@hku.hk
M. Mao, G. Cheng, C.-M. Che
HKU Shenzhen Institute of Research and Innovation
Shenzhen, Guangdong 518053, P. R. China

D. Zhang, L. Duan
Key lab of Organic Optoelectronics and Molecular Engineering of Ministry of Education
Department of Chemistry
Tsinghua University
Beijing 100084, P. R. China
E-mail: duanl@mail.tsinghua.edu.cn
P. An
School of Design
Southern University of Science and Technology
Shenzhen, Guangdong 518055, P. R. China
G. Cheng, C.-M. Che
Hong Kong Quantum AI Lab Limited
Unit 909-915 of 17W Building, Science Park, NT Hong Kong

The ORCID identification number(s) for the author(s) of this article can be found under https://doi.org/10.1002/adma.202311020

DOI: 10.1002/adma.202311020

However, due to their sophisticated device structure, these devices may face problems such as high fabrication costs, unsatisfactory device efficiency, and low operational stability. To date, no such CT-OLED with high operational stability has been reported. Alternatively, a simpler design in which multiple emitters are doped into a single-cell CT-OLED that can emit different colors at different driving voltages or currents has attracted considerable interest.[6,10,18] However, due to the inherent "color-aging" problem caused by the differential operational lifetime of each emitter in the emissive layer (EML),[7] such CT-OLEDs with high stability have rarely been reported for a long time. Recent advances have been made in the operational stability of such CT-OLEDs. Duan, Zhang, and co-workers used multiple TADF emitters to fabricate color-tunable white OLEDs with a wide color-temperature-tunability range, high EQE of 30.7%, and long operational lifetime LT_{80} (lifetime to 80% of an initial luminance) at an initial luminance (L_0) of 100 cd m^{-2} of over 20000 h.[5] Meanwhile, we proposed a CT-OLED utilizing monomers and aggregates of a single tetradentate Pt(II) emitter, which achieved a wide color span, high EQE of 23.23%, and long operational lifetime LT_{90} (time to 90% of an initial luminance)of almost 20000 h at L_0 of 100 cd m^{-2}.[19] However, since commercial monochromatic OLEDs have achieved high operational stability, longer operational lifetimes of CT-OLEDs are highly desirable in practical applications.

On the other hand, by using Pd(II) and Pt(II) phosphorescent molecular aggregates as emitters, stable OLEDs with high efficiency and long operational lifetimes at practical luminance were achieved. This is because these phosphorescent molecular aggregates possess high photoluminescence quantum yields (PLQYs), short excited state lifetimes, and high thermal stability.[1,20] Previously reported **Pd3o8-P** has a relatively long excited state lifetime (τ) and low photoluminescence (PL) efficiency at the monomer state, making it unsuitable as a single emitter for CT-OLEDs.[1] Ideally, monomers and aggregates of phosphorescent molecules used to fabricate CT-OLEDs should have high operational stability, short emission lifetime (τ), and high PLQYs in the monomer and aggregation states, where short τ is beneficial for the device's stability. Thus, designing a phosphorescent complex with short τ and high PLQY in both monomer and aggregation states remains a challenge.

In this study, we developed a modified Pt [O^N^C^N] (O^N^C^N = C–deprotonated 5, 5-dialkyl-2-(3-(pyridine-2-yl)-phenyl)−5H-indeno [1, 2-b] pyridine-9-olate) complex, **tetra-Pt-dbf**, and used it as a single light-emitting material to fabricate CT-OLED. This **tetra-Pt-dbf** complex achieves short τ and high PLQY in both monomer and aggregation states, resulting in a maximum EQE (EQE_{max}) of 30.2% in a device with 4 wt% dopant. When using a higher dopant concentration of 13 wt%, our CT-OLED achieves a large color-tuning range and high EQE_{max} of 28.1%. Furthermore, our CT-OLEDs exhibit low efficiency roll-off at high luminance, with EQE_{1000} (EQE at 1000 cd m^{-2}) of 27.8% and EQE_{10000} (EQE at 1000 cd m^{-2}) of 25.0%. We also achieve a wide color-tuning range using a more stable device structure with Commission Internationale de 1'Eclairage 1931 (CIE coordinates shifting from (0.510, 0.475) at 2.4 V to (0.379, 0.584) at 7.0 V. It is worth noting that by using commercial hosts, the LT_{90} of our device reaches over 500000 h at L_0 of 100 cd m^{-2}. To our best knowledge, this is the longest recorded operating lifetime of CT-OLEDs, more than 20 times longer than previous stable CT-OLEDs.[5,22] Furthermore, we demonstrated the potential application of our CT-OLED in the field of wearable biomedical sensor by designing a simple electromyography (EMG)-visualization system.

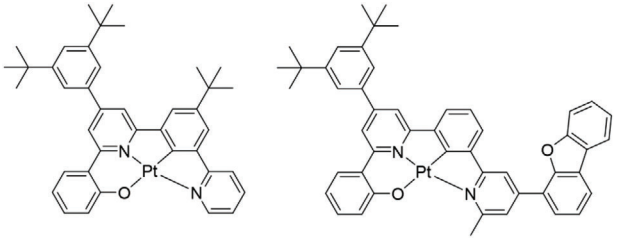

Scheme 1. Structures and selected performance data of **Pt-X-4** and **tetra-Pt-dbf**.

2. Results and Discussion

2.1. Synthesis and Characterization

Our previous work showed that [Pt (O^N^C^N)] complexes are susceptible to intermolecular Pt-Pt and/or ligand π-π interactions, which may lead to the formation of low energy light-emitting molecular aggregates.[21–23] We exploit the monomer emission and aggregation emission of **Pt-X-4** (depicted in **Scheme 1**) to fabricate high efficiency CT-OLEDs with the aim of avoiding color-aging limitations and promoting decent device stability.[22] This is because the device performance reported in public domain needs to be improved in practical applications such as terminal displays in lighting or sensing fields. To achieve high-efficiency CT-OLEDs with excellent operational stability, Pt complexes used in such devices should have (i) both high PLQY and short emission lifetime in both monomer and aggregate states to suppress efficiency roll-off and reduce degradation of the Pt complex under operating conditions and (ii) has good chemical and thermal stability to facilitate device fabrication and operational stability. To this end, we designed and synthesized a new platinum complex (**tetra-Pt-dbf**). As shown in Scheme 1 and Scheme S1 (Supporting Information), we attached dibenzofuran on the pyridyl ring to the [O^N^C^N] ligand scaffold in order to enhance the stability of the resulting Pt complex in aggregation form; the methyl group attached to the terminal pyridine is designed to promote the sublimation and increase the solubility of the complex **tetra-Pt-dbf**. The planar rigid dibenzofuran unit attached to the 4-position of the pyridyl ring is expected to induce strong molecular aggregation and reduce non-radiative decay channels by suppressing molecular vibrations, resulting in highly

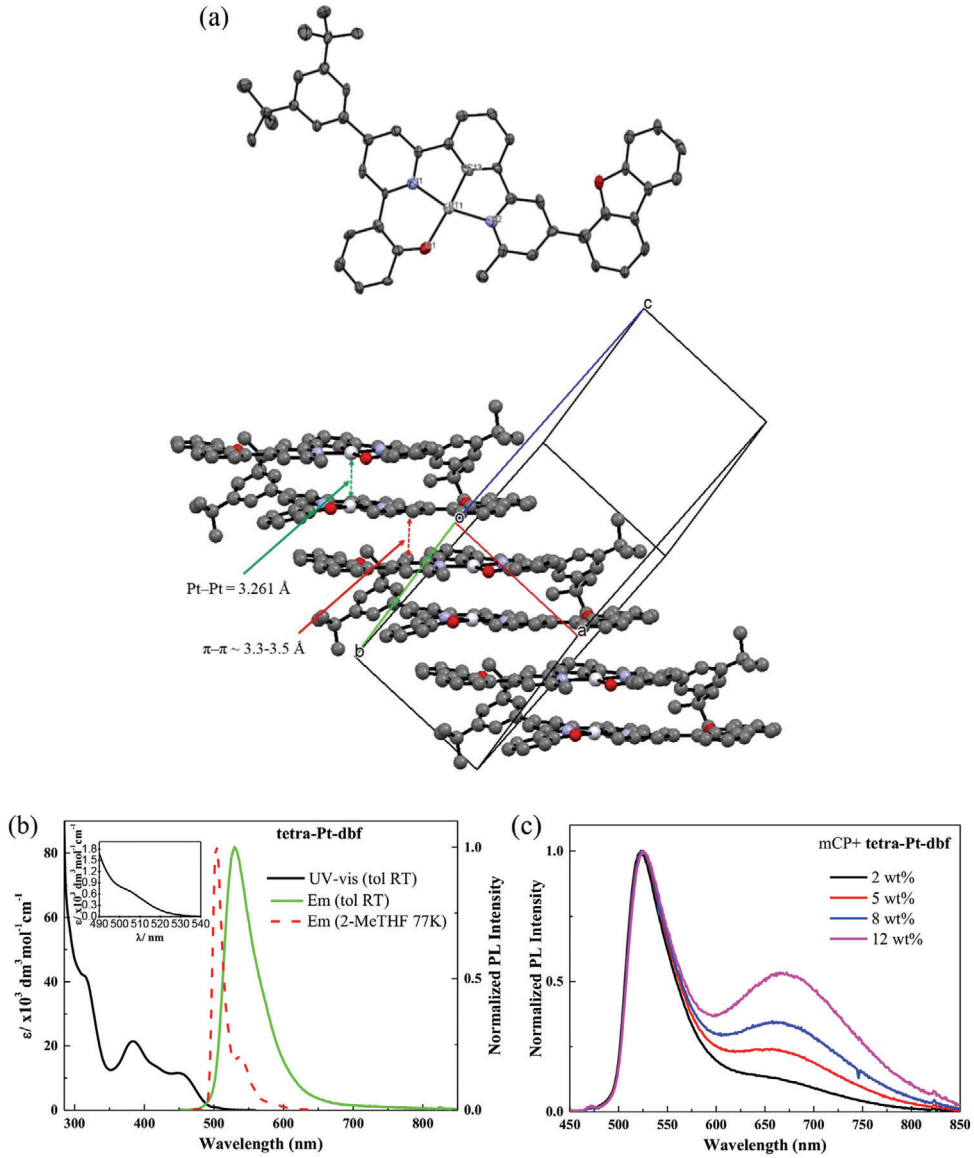

Figure 1. a) X-ray crystal structure and perspective view of **tetra-Pt-dbf** with omission of hydrogen atoms (thermal ellipsoid probability level: 30%); b) UV–vis absorption and emission spectra of **tetra-Pt-dbf** (2×10^{-5} M) in toluene at room temperature and in 2-MeTHF at 77 K; Inset magnifies absorptions at 490—540 nm. c) Emission spectra of **tetra-Pt-dbf** in mCP films with different doping concentrations (2 to 12 wt%); d) Calculated MOs diagrams of the structurally optimized **tetra-Pt-dbf** monomer and dimer in the T_1 excited state and the EDA calculation results of the [**tetra-Pt-dbf**]$_2$ dimer based on the X-ray crystal structure. For EDA calculation results, the total bonding energy (E_{Int}) is decomposed into different interaction energy terms: $E_{Int} = E_{Dimer} - 2E_{Monomer} = E_{Disp} + E_{Orb} + E_{Pauli} + E_{Elst}$.

efficiency aggregation emission. The Pt(II) complexes were characterized by ^{1}H and ^{13}C nuclear magnetic resonance (NMR) spectroscopy, high resolution mass spectrometry (HRMS) and elemental analysis.

The thermal stability of **tetra-Pt-dbf** was studied by thermogravimetric analysis. The decomposition temperature T_d of this complex is 508 °C (depicted in Figure S2, Supporting Information) (T_d defined as 5 wt% loss), showing the excellent thermal stability of **tetra-Pt-dbf**. Compared to the previous single emitter **Pt-X-4** (T_d = 430 °C),[24] **tetra-Pt-dbf** has higher T_d 508°C, indicating dibenzofuran substitution probably enhanced thermal stability of the Pt emitter.

The X-ray crystal structure of **tetra-Pt-dbf** is shown in **Figure 1**a, while selected bond lengths, bond angles, and crystallographic data are summarized in Tables S2.1–S2.2 (Supporting Information). Two **tetra-Pt-dbf** molecules are aligned in a head-to-head orientation with a Pt–Pt distance of 3.261 Å. Notably, intermolecular π–π interactions between each pair of **tetra-Pt-dbf** molecules can be observed in the crystal structure with interplanar distances of ≈3.3–3.5 Å.

The electrochemical properties of **tetra-Pt-dbf** were studied by cyclic voltammetry (CV) in *N,N-dimethylformamide* (DMF), and the electrochemical data are shown in Figure S1 (Supporting Information). For this complex, a reduction peak at −1.58 V (E_{red})

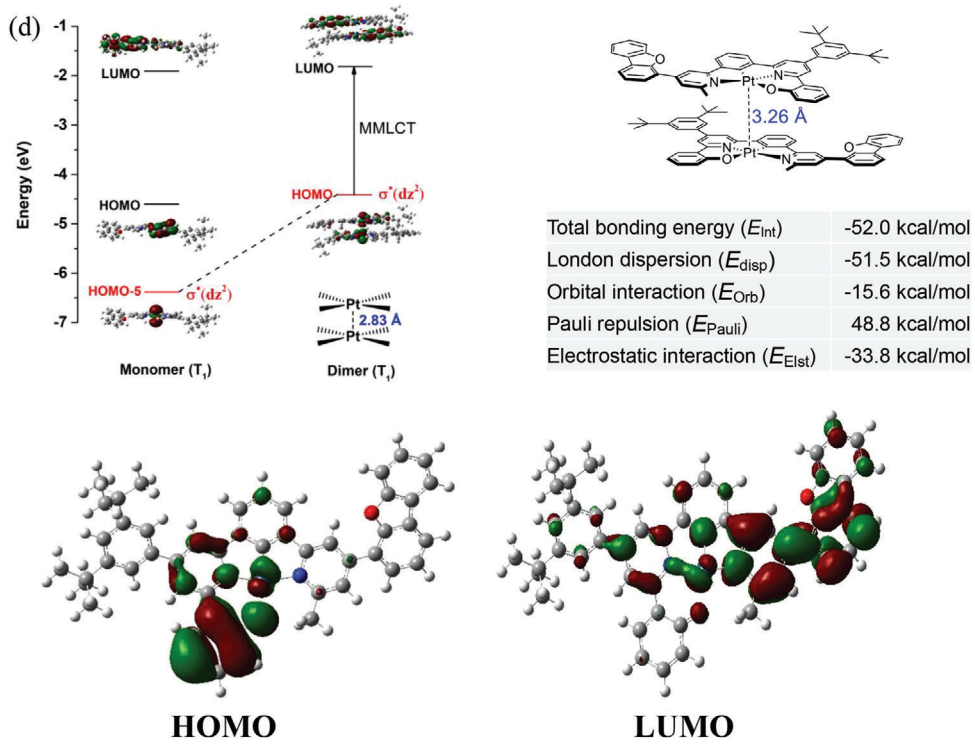

Figure 1. *Continued*

and an irreversible oxidation wave at 0.79 V (E_{ox}) were observed. Both the reduction couple and the irreversible oxidation wave are attributed to the ligand-centered reactions of the OˆNˆCˆN moiety.[23] The highest occupied molecular orbital (HOMO) and lowest unoccupied molecular orbital (LUMO) levels of this complex were estimated from the onset oxidation potentials and reduction potentials at −5.12 eV and −2.74 eV, respectively (summarized in Table S1, Supporting Information).

The photophysical data of **tetra-Pt-dbf** are summarized in Table S1 (Supporting Information). Figure 1b depicts the UV-visible absorption spectrum of this complex in toluene solution. The intense absorption band ($\epsilon > 4 \times 10^4$ $dm^3mol^{-1}cm^{-1}$) at wavelength below 320 nm corresponds to intra-ligand (IL)[1] π-π^* transitions of the OˆNˆCˆN ligand. Relatively weak absorption beyond ≈400 nm ($\epsilon = (0.076–1.2) \times 10^4$ $dm^3mol^{-1}cm^{-1}$) can be assigned to mixed singlet intra-ligand charge-transfer (^{1}ILCT) and singlet metal-to-ligand charge-transfer (^{1}MLCT) transitions. **Tetra-Pt-dbf** exhibits strong yellowish green (λ_{max} = 529 nm) emission in deoxygenated toluene, with an emission lifetime τ of 2.44 µs and emission quantum yield as high as 0.82 (Figure 1b). This structureless yellowish green emission band (λ_{max} = 529 nm) of **tetra-Pt-dbf** indicates that the emitting excited state has mixed ^{3}MLCT/^{3}ILCT parentage, as previously reported.[23,24] Different concentrations of **tetra-Pt-dbf** were also doped into mCP films to study the solid-state photo-physical properties of this complex. As shown in Figure 1c, all films show strong emission with λ_{max} ranging from 523 nm (2 wt%) to 526 nm (12 wt%), which is attributed to the monomer emission of **tetra-Pt-dbf**.[21] However, as the doping concentration increases from 2 wt% to 12 wt%, another low-energy emission (λ_{max} = 657–665 nm) gradually develops, which is assigned to the triplet metal-metal-to-ligand charge transfer (^{3}MMLCT) emission of the aggregate species.[1,20,21,25] The **tetra-Pt-dbf**/mCP film shows high PLQY (0.66 at 12 wt%, 0.87 at 2 wt%), and shorter τ of the 523–526 nm (τ = 2.10–1.34 µs) and 657–667 nm (τ = 1.61–1.13 µs) emission bands (summarized in Table S1, Supporting Information), showing good photoluminescence properties in both monomer and aggregated states.

Compared with the t-butyl unit of previous complex **Pt-X-4**, the planar rigid dibenzofuran unit of **tetra-Pt-dbf** will help induce intermolecular aggregation. We believe that the stability of solid-state complexes is closely related to the intermolecular interactions and performed Energy decomposition analysis (EDA) on [**tetra-Pt-dbf**]$_2$ dimer. The EDA results show that the [**tetra-Pt-dbf**]$_2$ dimer has a strong intermolecular bonding energy of −52.0 kcal mol^{-1} (depicted in Figure 1d). The bonding interactions are largely contributed by the London dispersion interaction (−51.5 kcal mol^{-1}), suggesting strong π-π stacking between molecules. The large intermolecular bonding energy is beneficial to the formation of stable **tetra-Pt-dbf** aggregates. We performed Density functional theory (DFT) and time-dependent density functional theory (TD-DFT) calculations to study the photo-physical properties of **tetra-Pt-dbf**. We optimized the ground state S_0 structure and lowest triplet excited state T_1 structure of dimer [**tetra-Pt-dbf**]$_2$. Calculations for the dimer [**tetra-Pt-dbf**]$_2$ show that the Pt-Pt distance at T_1 (2.83 Å) is reduced compared to S_0 (3.30 Å). The molecular orbital (MO) diagrams of monomer **tetra-Pt-dbf** and dimer [**tetra-Pt-dbf**]$_2$ with the optimized structure of T_1 state are shown in Figure 1d. For monomer **tetra-Pt-dbf**, the Pt-5dz^2 orbital is HOMO-5. After dimerization, the short Pt-Pt contact distance in the T_1 state of [**tetra-Pt-dbf**]$_2$ results in a large energy splitting between the two

Table 1. Selected performances of OLEDs reported in this work with different concentrations of **tetra-Pt-dbf**.

Device No.	[conc.]	Turn-on[a] [V]	L_{max}[b] [cd m^{-2}]	EQE_{max} [%]	PE_{max}[c] [lm W^{-1}]	CIE [x,y][d]		Lifetime [hour]	
						at 2.8V	at 7V	$LT_{90@1000}$[e]	$LT_{90@100}$[f]
1	4%	2.4	148300	30.2	94.1	(0.342, 0.618)	(0.332,0.607)	/	/
	7%	2.4	139700	28.9	72.5	(0.421,0.558)	(0.339,0.605)	/	/
	10%	2.4	131000	28.8	57.2	(0.442,0.542)	(0.421,0.558)	/	/
	13%	2.4	106800	28.1	49.6	(0.479,0.508)	(0.449,0.533)	/	/
2	4%	2.5	72329	17.4	69.8	(0.347,0.618)	(0.332,0.607)	951	53478
	7%	2.5	51044	17.2	68.3	(0.441,0.542)	(0.406,0.563)	1383	77772
	10%	2.5	41523	16.3	49.4	(0.476,0.510)	(0.434,0.541)	672	37789
	13%	>2.5	35749	15.5	21.9	(0.501,0.480)	(0.455,0.521)	658	37002
3		2.4	150960	17.2	30.4	(0.510,0.475)	(0.379,0.584)	9288	520536

[a] Voltage at the luminance of 1 cd m^{-2}; [b] Maximum luminance; [c] Maximum power efficiency; [d] Commission Internationale de l'Eclairage 1931 coordinates; [e] Time to 90% of the initial luminance of 1000 cd m^{-2}; [f] Time to 90% of the initial luminance of 100 cd m^{-2}.

Pt 5dz^2 orbitals. Such a large energy splitting lifts the σ^*(5dz^2) orbital to become HOMO in the dimer [**tetra-Pt-dbf**]$_2$. LUMO is mainly localized on the ligand. Therefore, the excited state of **tetra-Pt-dbf** aggregates is ^{3}MMLCT (metal-metal-to-ligand charge transfer) in nature, which is consistent with other reported Pt(II) complexes.[20,21,25] The emission energy of dimer [**tetra-Pt-dbf**]$_2$ in the T_1 state is calculated to be 1.67 eV, which is consistent with the experimentally observed emission energy of 1.77 eV for OLED devices. In order to investigate the role of dibenzofuran units in **tetra-Pt-dbf** molecules, we calculated and compared the frontier molecular orbitals of **tetra-Pt-dbf** and **Pt-ref** in the optimized T_1 state. The LUMO of **tetra-Pt-dbf** extends significantly to the dibenzofuran unit (as illustrated in Figure 1d) and is more delocalized than **Pt-ref** (as illustrated in Figure S13, Supporting Information).

2.2. Device Performance

The short τ and excellent PLQY of **tetra-Pt-dbf** in both monomer and aggregation states motivated us to investigate its electroluminescent (EL) properties using CT-OLED structures. We fabricated vacuum-deposited OLEDs (Device 1) with ITO/HAT-CN (5 nm)/TAPC (30 nm)/SF-BCZ (10 nm)/SF-BCZ: SF-TRZ: **tetra-Pt-dbf** (x wt%) (30 nm)/SF-TRZ (10 nm)/DPPyA (30 nm)/LiF (1.2 nm)/Al (150 nm) architecture, where x represents the dopant concentration of 4, 7, 10, and 13 wt%, respectively. In these devices, we use HAT-CN (1, 4, 5, 8, 9, 11-hexaazatriphenylene hexacarbonitrile) and LiF as the hole-injecting layer and electron-injecting layer, respectively. TAPC (1, 1-bis-(4-bis(4-methyl phenyl)-amino-phenyl)-cyclohexane) and DPPyA (9,10-bis(6-phenylpyridin-3-yl)anthracene) are used as the hole-transporting layer (HTL) and electron-transporting layer (ETL), respectively. SF-BCZ (9-(9,9′-spirobi[fluoren]−3-yl)−9′-phenyl-9H,9′H-3,3′-bi-carbazole) and SF-TRZ (2-(3′-(9,9′-spirobi[fluoren]−3-yl)-[1,1′-biphenyl]−3-yl)−4,6-diphenyl-1,3,5-triazine) are used as the electron-blocking layer (EBL) and hole-blocking layer, respectively. We employed a mixture of SF-BCZ/SF-TRZ with a weight ratio of 1:1 as co-host in the emissive layer (EML). **Figure 2f** depicts the schematic device structure of the energy level alignment of each layer.

At a low doping concentration of 4 wt%, the EL spectrum (depicted in Figure 2a) shows a single peak at 525 nm, which we assign to the **tetra-Pt-dbf** monomer emission (compared with the PL spectrum shown in Figure 1b). These EL spectra remain consistent as the luminance increases from 100 to 10000 cd m^{-2}, keeping the CIE coordinates ≈(0.342, 0.618) (deviation (± 0.01, ± 0.01)). However, as the dopant concentration increases from 7 wt% to 13 wt%, a new emission peak appears at ≈670 nm, which we attribute to the **tetra-Pt-dbf** aggregated emission (^{3}MMLCT)[19,21] based on the PL emission shown in Figure 1b. Thus, for Device 1, a minimum doping concentration of 7 wt% is required to show color tunability. Interestingly, in Figure 2d, the color-tunability phenomenon can be clearly observed in the device with a doping concentration of 13 wt%, showing the CIE coordinates changing from (0.479, 0.508) at 100 cd m^{-2} to (0.449, 0.533) at 100000 cd m^{-2} (see **Table 1**). According to our previous work, the voltage-dependent color-tunability phenomenon is attributed to the shift of the recombination zone and the competition between charge-trapping and direct energy transfer mechanisms.[22] As shown in Figure 2e, these devices exhibit high efficiency and low efficiency roll-off in the luminance range of 1000–10000 cd m^{-2}. Among them, the device with 4 wt% **tetra-Pt-dbf** has the highest EQE_{max} of 30.2%. Even at high luminance of 1000 and 10000 cd m^{-2}, the device's EQE remains at 30.0% and 27.8%, respectively. Maximum luminance is as high as 148300 cd m^{-2} (summarized in Table 1). At the same time, the aforementioned device containing 13 wt% **tetra-Pt-dbf** not only has a wide color-tuning range, but also exhibits a high EQE_{max} of 28.1% and low efficiency roll-off at high luminance of 1000 (EQE_{1000} of 27.8%) and 10000 cd m^{-2} (EQE_{10000} of 25.0%). This CT-OLED is one of the most efficient CT-OLEDs with EQE_{max} up to ≈30%,[5] which is better than other reported CT-OLEDs.[6,20,22] We infer that such high EL efficiency of Device 1 with 13 wt% dopant could be attributed to the high PLQY of the emitter **tetra-Pt-dbf** in both the monomer and aggregation states. Furthermore, good energy level alignment from ETL to EML could reduce energy barriers and prevent relevant quenching. The short excited-state lifetime and high thermal stability of **tetra-Pt-dbf** also help to suppress triplet-related annihilation or thermal degradation, thereby suppressing efficiency roll-off at high luminance.[29] As mentioned in Section 2.1, the PLQY of **tetra-Pt-**

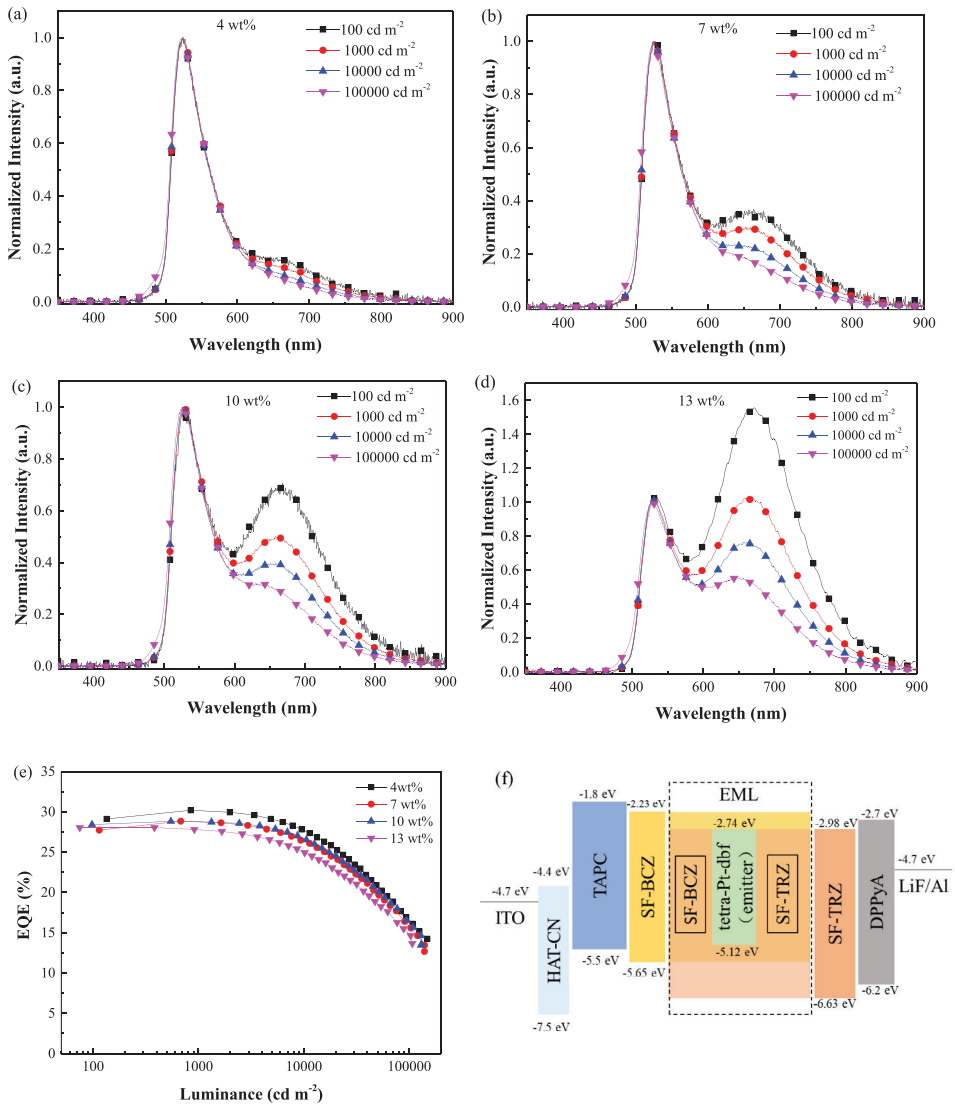

Figure 2. Normalized EL spectra of Device 1 with a) 4 wt%, b) 7 wt%, c) 10 wt%, and d) 13 wt% dopant concentration at the indicated luminance, ranging from 100 to 100000 cd m^{-2}. e) Luminance-EQE curves of Device 1 with different doping concentrations. f) Schematic diagram of device structure with proposed energy level diagram.

dbf/mCP films was 0.87 at 2 wt% and 0.66 at 12 wt%, respectively. This means that the EQE_{max} of a device with high dopant concentration (≈12 wt%) would be much lower than that of a device with low dopant concentration (≈2 wt%). But the EQE_{max} of Device 1 with 13 wt% dopant is as high as 28.1%, which is comparable to the EQE_{max} of Device 1 with 4 wt% dopant (30.2%). In general, the EQE value is mainly determined by PLQY of the emitter and the out-coupling efficiency of the device. The horizontal transition dipole moment can significantly improve the out-coupling efficiency. Since aggregates of planar Pt(II) molecules are more likely to adopt a horizontal emitting dipole orientation,[1,20,21] we infer that the out-coupling efficiency and EQE_{max} are improved for Device 1 with 13 wt% dopant, because of the aggregates formed in the EML of the device. Therefore, this device was found to exhibit a similar EQE_{max} to Device 1 with 4 wt% dopant.

To evaluate the stability of the device in practical use, we measured the operational lifetime of the CT-OLED using **tetra-Pt-dbf** as light-emitting dopant under common laboratory conditions. We used a modified device structure (Device 2) with the following architecture: ITO/HAT-CN (5 nm)/BPBPA (120 nm)/FSF4A (10 nm)/SF-BCZ: SF-TRZ: **tetra-Pt-dbf** (y wt%) (20 nm)/ANT-BIZ (10 nm)/ANT-BIZ: Liq 50 wt% (40 nm)/Liq (1.2 nm)/Al (100 nm), where y represents the dopant's concentration of 4, 7, 10, and 13 wt%, respectively. BPBPA (N4, N4, N4′, N4′-tetra([1,1′-biphenyl]−4-yl)-[1,1′-biphenyl]−4,4′-diamine) and ANT-BIZ (1-(4-(10-([1,10-biphenyl]−4-yl) anthracene-9-yl)phenyl)−2-ethyl-1H-benzo[d]-imidazole) were used as HTL and ETL, respectively. FSF4A (N-([1, 10-biphenyl]−2-yl)-N-(9, 9-dimethyl-9H-fluoren-2-yl)−9, 90-Spirobi [9H-fluoren]−4-amine) as the EBL, and Liq (8-hydroxy-quinolinatolithium) as the electron-injecting layer and also doped in the ET. Notably, we

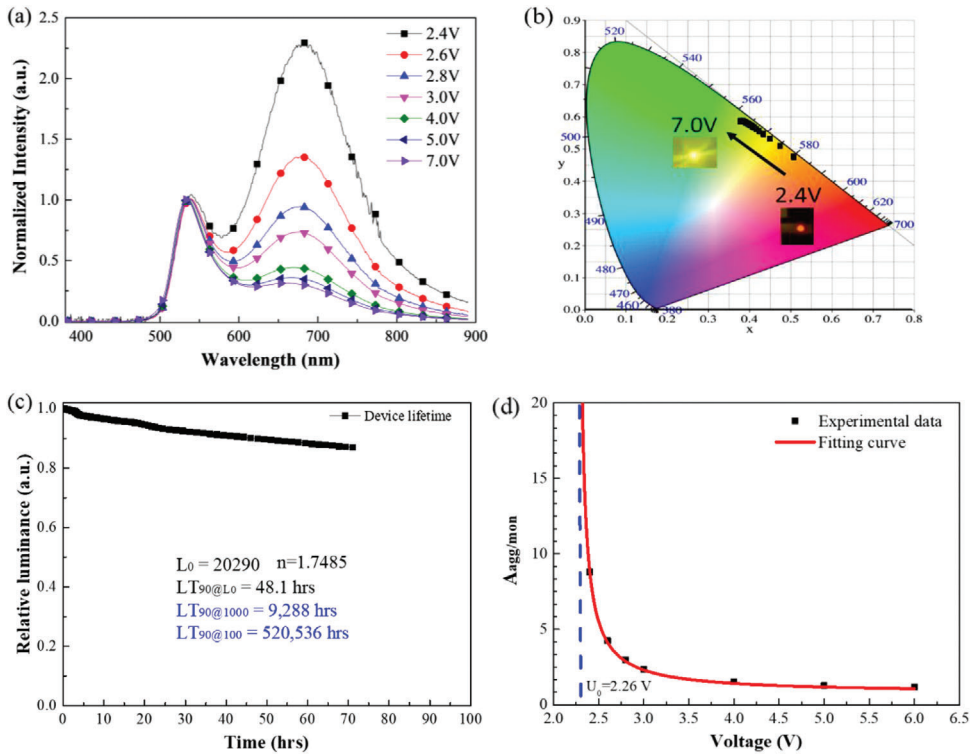

Figure 3. a) Normalized EL spectra of Device 3 with 7 wt% dopant concentration from 2.4 V to 7.0 V; b) CIE coordinates shift of Device 3 from 2.4 V to 7.0 V; c) plots of relative luminance-operational lifetime at a constant current density of 60 mA cm^{-2}; d) the dependence of $A_{agg/mon}$ on driving voltage of Device 3 with a **tetra-Pt-dbf** emitter; the solid squares represent experimental data; the solid red line represents theoretical fitting results, and the blue dashed line indicates the build-in voltage.

employed a 120-nm-thick BPBPA layer to effectively balance the charged carriers and prevent thermoelectric breakdown during long-term device lifetime testing. These devices displayed color-tunable EL spectra (depicted in Figure S5, Supporting Information), good efficiency and operational stability, as shown in Table 1. These devices have EQE above 15% and a LT_{90} beyond 37000 h at L_0 of 100 cd m^{-2}. Among these devices, assuming a degradation acceleration factor n of 1.75, the longest estimated LT_{90} for a device with 7 wt% doping concentration is 77772 h at L_0 of 100 cd m^{-2}. When the doping concentration is increased to 10 wt%, a moderate color-tuning range and a long operational lifetime can be achieved. The CIE coordinates shift from (0.476, 0.510) at 2.8 V to (0.434, 0.541) at 7 V, and the LT_{90} is as long as 37789 h.

To further improve the operational lifetime of CT-OLEDs, we employed an alternate "p-i-n" device structure (Device 3, Figure S6, Supporting Information) and commercial host materials (Host 1 and Host 2) under common laboratory conditions. Some chemical structures are described in detail in Figure S7 (Supporting Information). **Figure** 3a shows the different EL spectra of Device 3 with a dopant concentration of 7 wt% at driving voltages from 2.4 to 7.0 V. At low voltages from 2.4 and 2.6 V, the aggregation emission of **tetra-Pt-dbf** (peaked at ≈670 nm) dominates, and as the voltage increases, the steadily enhanced monomer emission (peaked at 525 nm) gradually dominates. A wide color-tuning range is achieved, with CIE coordinates shifting from (0.510, 0.475) at 2.4 V to (0.379, 0.584) at 7.0 V (see Table 1 and Figure 3b). More importantly, at an initial L_0 of 20290 cd m^{-2}, the operational lifetime LT_{90} was measured to be 48.1 h (Figure 3c). Utilizing the exponential decay model[26] (the degradation acceleration factor (n) is calculated as 1.7485, illustrated in Figure S6c, Supporting Information), the LT_{90} at 10000 cd m^{-2}, 1000 cd m^{-2}, and 100 cd m^{-2} is estimated to be 166 h, 9288 h, and 520536 h, respectively, which are more than 20 times longer than the state-of-the-art CT-OLEDs[5,19] and even comparable to most reported monochromatic stable OLEDs.[1,3,27–31] Compared with other reported CT-OLEDs or our previous CT-OLED using **Pt-X-4** ($LT_{90@100}$ = 19105 h) (summarized in Table S6, Supporting Information), this CT-OLED using our modified **tetra-Pt-dbf** shows superior device stability. Given that lifetime measurements are performed under constant current conditions, the driving voltage increases with device degradation, resulting in color shifts due to the inherent color tunability of the device. To address this issue, driving voltage and CIE coordinates measurements were performed on both the fresh device and the device for the lifetime measurement (LT_{90}). As shown in Figure S9 and Table S3 (Supporting Information), for a constant driving current density of 30 (or 60 mA cm^{-2}), the driving voltage was found to exhibit only a slight increase of 0.6 (or 0.4 V), resulting in a negligible shift of 0.008 (or 0.004) in CIEx and 0.006 (or 0.004) in CIEy, respectively. On the other hand, considering the long estimated Device 3 operational lifetime ($LT_{90@100}$ = 520536 h), no significant device degradation is expected to occur during practical use of our CT-OLEDs at low luminance of 100 cd m^{-2}. Therefore, long-term operation is unlikely to compromise the color-tunable capability of our device. In addition to the stability

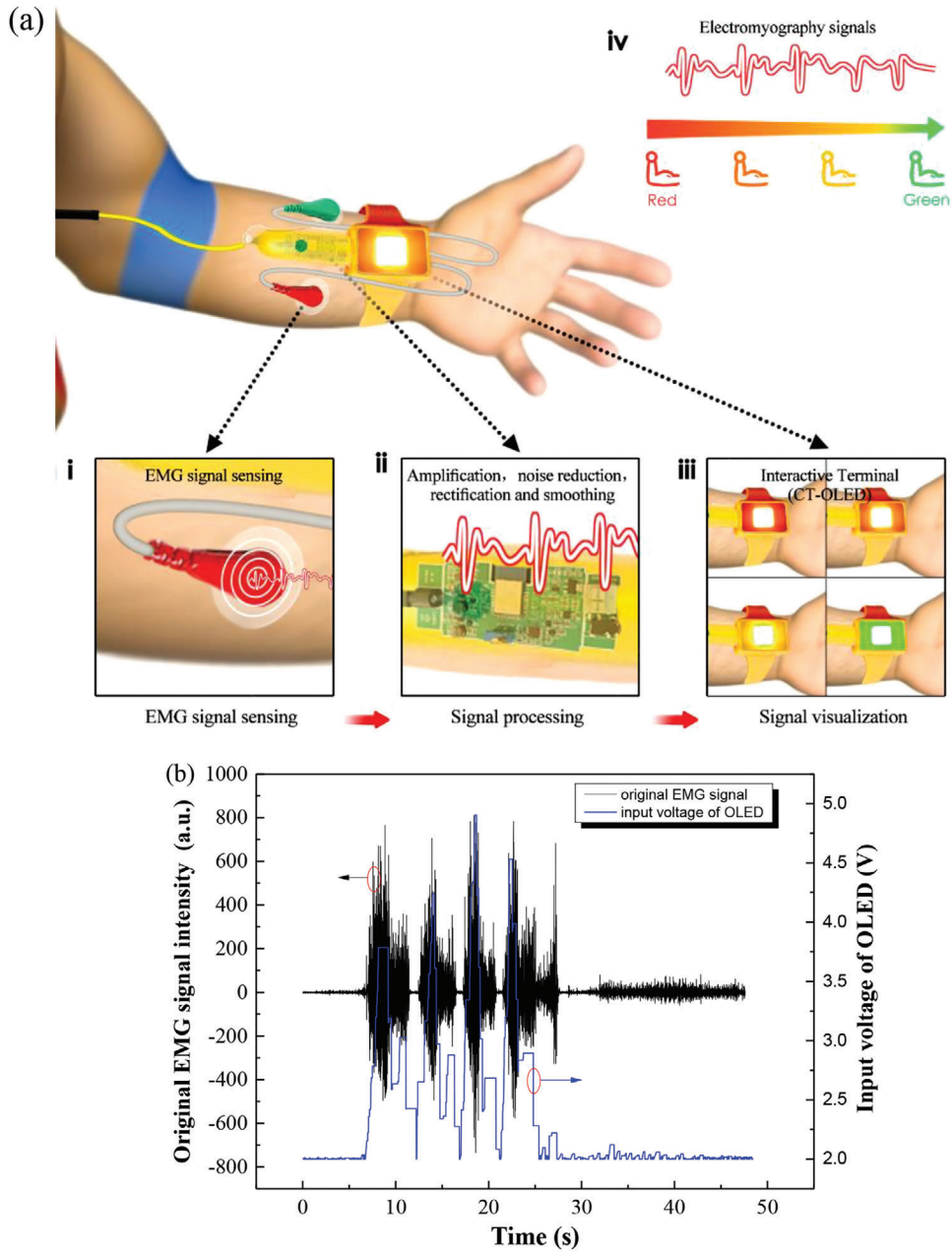

Figure 4. a) Schematic illustration of EMG-visualization system with CT-OLED; b) the Time-Original EMG signal-real-time input voltage curves of our EMG-visualization systems.

factors of commercial host materials, the excellent operational stability of this CT-OLED is first attributed to the short excited state lifetime of **tetra-Pt-dbf** in the monomer and aggregation states ($\tau < 2\ \mu s$). Phosphorescent metal-organic emitters usually have short triplet excited state lifetimes due to "heavy atom effect", which promotes rapid radiative decay from the triplet excited state to the ground state. This suppresses triplet-related annihilation to a large extent, which not only reduces efficiency roll-off at high current density, but also extends device lifetime.[2,26] Both the monomer and aggregate state emission of **tetra-Pt-dbf** have short excited state lifetimes, which is different from other complexes[1,20] that only have short excited state lifetimes in the monomer or aggregated state. Therefore, our CT-OLED using a single light-emitting material **tetra-Pt-dbf** can simultaneously achieve both monomer (high-energy band) emission and aggregation (low-energy band) emission, with a short excited state lifetime, thus extending the device's lifetime. The modified **tetra-Pt-dbf** has higher thermal stability (T_d = 508 °C) compared to the previous emitter **Pt-X-4** (T_d = 430 °C). As a result, devices fabricated using **tetra-Pt-dbf** have reduced thermal degradation, thereby enhancing stability.[2] Moreover, compared to the dimer of previous **Pt-X-4** (E_{int} = −44.2 kcal mol^{-1}, listed in Table S4,

Supporting Information), the [**tetra-Pt-dbf**]$_2$ dimer has a higher intermolecular bonding energy (E_{int} = −52.0 kcal mol^{-1}) due to the strong intermolecular π-π stacking interaction, which indicates that the **tetra-Pt-dbf** aggregates have relatively higher chemical stability, and may better inhibit the decomposition of **tetra-Pt-dbf** aggregates in OLED devices. In addition, unlike other CT-OLEDs that use multiple emitters, our single-emitter CT-OLEDs can basically avoid the "color-aging issue" (see Figure S10, Supporting Information)[7] and eliminate quenching between different doped species in an EML, thereby extending the operational lifetime. Our CT-OLED is doped with a single **tetra-Pt-dbf** emitter and features a wide color-tuning range, high EQE, low efficiency roll-off and superior operational stability. This suggests that CT-OLEDs using planar luminescent Pt(II) complexes as single emitters have broad application prospects, such as in smart lighting, decoration, and wearable biomedical sensors.[5,6,8]

In order to better explain the mechanism of this excellent color tunability performance, we adopt the classical "trapping and energy-transfer" model[18] to simulate the experimental data; this model can be expressed by Equation (1).

$$q(U) = \frac{D}{\mu}\left(\frac{d}{L_T}\right)^2 \frac{1}{U - U_0} + \frac{d}{L_T} \quad (1)$$

Equation (1) was derived by Meerholz and co-workers[18] for single-layer polymer OLEDs and applied to multilayer OLEDs by Wang and coworkers[32] to explain CT-OLEDs. Here we use the integral area ratio of aggregation/monomer ($A_{agg/mon}$) (acquired via "Guass" fitting) instead of the intensity ratio of each emission band in the previous literature,[18,32] to describe emission ratio q(U) in Equation (1). This is because the aggregation emission band has a larger full width at half maximum (FWHM) compared to the monomer emission band, which may lead to a severe bias in the simulation if intensity ratio is used to describe q(U). In Equation (1), D is the diffusion coefficient of trapped electrons, μ is the mobility of carriers, d is the thickness of EML, L_T is the average diffusion distance before carriers reach the trapping center, U is the driving voltage, and U_0 is the built-in electronic field. D/μ is the Einstein relation describing the ratio between diffusivity and mobility. Equation (1) was used to fit the experimental data. The curve fitting matches the experimental data with a correlation coefficient R^2 of 0.996, as shown in Figure 3d. Here, we obtain a built-in field U_0 of 2.26 V and an Einstein relation D/μ of 2.0, which is close to the values reported in conventional organic systems.[18] The high agreement between the experimental data and the fitting curve indicates that this color-tunability phenomenon may arise from the competition between charge trapping and direct energy transfer to the emitter.

As a potential application, we have also initially explored the potential application of CT-OLED in the field of wearable biomedical sensors. We designed an EMG-visualization system, including a power control module, EMG sensing electrodes, signal processing module (including noise reduction, signal amplification, rectification and smoothing), and an integrated circuit with our CT-OLED user interaction terminal (as shown in **Figure 4a**). The retrieved EMG analog signal is processed through signal amplification and noise reduction, and then converted into an amplified direct current (DC) analog signal (voltage signal) through signal rectification and smoothing; then this DC analog signal is converted into DC digital signal via Analog-to-Digital Converter (ADC). This DC digital signal then is transmitted to Microcontroller Unit (MCU), which will modulate the load of circuit and instantly control the input DC-voltage of the CT-OLED, ranging from 2.0 to 5.0 V. (More details are described in Figure S8, Supporting Information) The CT-OLED subsequently emits different colors, shifting from red via orange and yellow to yellowish green. As a result, the invisible EMG signal is instantly visualized into a visible varied-color signal in real time (as shown in Figure 4b). Since the CT-OLED described here has high efficiency and excellent operational stability, we conceive that better EMG-vision sensors with superior flexible electrodes can be fabricated; our stable CT-OLED and high-reliability flexible electrodes will significantly enhance the operational stability of such EMG sensors.

3. Conclusion

High efficiency, small efficiency roll-off, wide color-tuning range, and long operational lifetime at practical luminance are key attributes for CT-OLED applications. By carefully designing the molecular structure of Pt(II) emitter and device architecture, high EQE of ≈30%, low efficiency roll-off, and a wide color-tuning range are achieved. Moreover, by adopting a "p-i-n" structure and commercial host, our single-emitter **tetra-Pt-dbf** CT-OLED has been shown to have an ultra-long operational lifetime of $LT_{90@100}$ > 500000 h (as the interactive terminal of sensors, the CT-OLED can function at ≈100 cd m^{-2}). Such excellent device performance demonstrated by our single-emitter CT-OLED indicates that CT-OLED can be a viable candidate for interactive terminals in intelligent lighting and wearable sensor applications. Our rough and ready EMG-visualization system provides a potential option for CT-OLED applications in wearable biomedical sensors, which will be discussed in our future work.

Supporting Information

Supporting Information is available from the Wiley Online Library or from the author.

Acknowledgements

M.M. and H.L. contributed equally to this work. This work was supported by the Guangdong Major Project of Basic and Applied Basic Research (21019B030302009), Mainland-Hong Kong Joint Funding Scheme (MHP/134/22), Innovation and Technology Fund (ITS/224/17FP), and Hong Kong Quantum AI Lab Limited, AIR@InnoHK of Hong Kong Government, Science Technology and Innovation Commission of Shenzhen Municipality (JCYJ20200109150414471, JCYJ20180508162429786), and International Science and Technology Cooperation Program of Jiangsu Province (Grant No. BZ2023059). The authors thank Dr. Lei Dai and Mr. Lei Pei of Aglaia Corp. for testing the device's lifetime, and thank Dr. Tsz-Lung Lam of Chem. Dept., the University of Hong Kong for testing the photophysical data of the Pt(II) complex. The authors also thank Dr. Jiechen Yin, Mr. Cirui Zhang of Lettin Corp. and Dr. Shuai-jian Yang of Biomedical Engineering Dept., Southern University of Science and Technology for fabricating the driving circuit of the EMG-visualization system.

Conflict of Interest

The authors declare no conflict of interest.

Data Availability Statement

The data that support the findings of this study are available from the corresponding author upon reasonable request.

Keywords

color-tunable, device lifetime, OLED, platinum complex, wearable biomedical device

Received: October 22, 2023
Revised: January 29, 2024
Published online: March 30, 2024

[1] L. Cao, K. Klimes, Y. Ji, T. Fleetham, J. Li, *Nat. Photonics* **2021**, *15*, 230.
[2] S.-S. Swayamprabha, D.-K. Dubey, *Adv. Sci.* **2020**, *8*, 2002254.
[3] S. O. Jeon, K. H. Lee, J. S. Kim, S.-G. Ihn, Y. S. Chung, J. W. Kim, H. Lee, S. Kim, H. Choi, J. Y. Lee, *Nat. Photonics* **2021**, *15*, 208.
[4] S. Lee, M. S. Sim, S.-Y. Kwak, H. Koo, S. Kim, S. Hong, K. Y. Hwang, J. Yi, S. Park, Y. Kwak, H. Choi, B. L. Lee, O. Kwon, B. Choi, S. H. Kim, *SID 2020 Digest.* **2020**, *51*, 281.
[5] C. Zhang, D. Zhang, Z. Bin, Z. Liu, Y. Zhang, H. Lee, J. H. Kwon, L. Duan, *Adv. Mater.* **2022**, *34*, 2103102.
[6] S. Ying, Y. Wu, Q. Sun, Y. Dai, D. Yang, X. Qiao, J. Chen, D. Ma, *Appl. Phys. Lett.* **2019**, *114*, 033501.
[7] S. Pan, K. Liu, Z. Ling, K. Guo, S. Wang, M. Chen, C. Si, Z. Tang, B. Wei, *Surf. & Coat. Tech.* **2019**, *363*, 442.
[8] J. H. Koo, S. Jeong, H. J. Shim, D. Son, J. Kim, D. C. Kim, S. Choi, J.-I. Hong, D.-H. Kim, *ACS Nano* **2017**, *11*, 10032.
[9] C. W. Joo, J. Moon, J. H. Han, J. W. Huh, J. Lee, N. S. Cho, J. Hwang, H. Y. Chu, J.-I. Lee, *Org. Electron.* **2014**, *15*, 189.
[10] G. Cheng, K. T. Chan, W.-P. To, C.-M. Che, *Adv. Mater.* **2014**, *26*, 2540.
[11] G. Mu, T. Rao, Y. Qi, S. Ma, Q. Hao, M. Chen, X. Tang, *Adv. Funct. Mater.* **2023**, *33*, 2301280.
[12] Y. Li, N. Liu, P. Zhou, W. Lan, H. Pu, Y. Liao, *Mater. Sci-Medzg.* **2021**, *27*, 264.
[13] Y. Zhao, R. Chen, Y. Gao, K. S. Leck, X. Yang, S. Liu, A. P. Abiyasa, Y. Divayana, E. Mutlugun, S. T. Tan, H. Sun, H. V. Demir, X. W. Sun, *Org. Electron.* **2013**, *14*, 3195.
[14] S. Liu, R. Wu, J. Huang, J. Yu, *Appl. Phys. Lett.* **2013**, *103*, 133307.
[15] Y. Jiang, J. Lian, S. Chen, H. S. Kwok, *Org. Electron.* **2013**, *14*, 2001.
[16] M. Y. Teng, Q. Xu, H. Y. Li, L. Wu, Y. X. Zheng, C. Lin, L. Wang, *RSC Adv.* **2012**, *2*, 10175.
[17] M. Fröbel, T. Schwab, M. Kliem, S. Hofmann, K. Leo, M. C. Gather, *Light Sci. Appl.* **2015**, *4*, e247.
[18] M. C. Gather, R. Alle, H. Becker, K. Meerholz, *Adv. Mater.* **2007**, *19*, 4460.
[19] M. Mao, T.-L. Lam, W.-P. To, X. Lao, W. Liu, S. Xu, G. Cheng, C.-M. Che, *Adv. Mater.* **2021**, *33*, 2004873.
[20] K. T. Ly, R. W. Chen-Cheng, H.-W. Lin, Y. J. Shiau, S. H. Liu, P. T. Chou, C. S. Tsao, Y. C. Huang, Y. Chi, *Nat. Photonics* **2017**, *11*, 63.
[21] G. Cheng, Q. Wan, W.-H. Ang, C. L. Kwong, W.-P. To, P. K. Chow, C. C. Kwok, C.-M. Che, *Adv. Optical. Mater.* **2019**, *7*, 1801452.
[22] M. Mao, J. Peng, T.-L. Lam, W.-H. Ang, H. Li, G. Cheng, C.-M. Che, *J. Mater. Chem.* **2019**, *7*, 7230.
[23] G. Cheng, S. C. F. Kui, W.-H. Ang, M. Y. Ko, P.-K. Chow, C. L. Kwong, C. C. Kwok, C. Ma, X. Guan, K. H. Low, S. J. Su, C.-M Che, *Chem. Sci.* **2014**, *5*, 4819.
[24] S. C. F. Kui, P.-K. Chow, G. Cheng, C. C. Kwok, C. L. Kwong, K. H. Low, C.-M. Che, *Chem. Commun.* **2013**, *49*, 1497.
[25] K. H. Kim, J. L. Liao, S. W. Lee, B. Sim, C. K. Moon, G. H. Lee, H. J. Kim, Y. Chi, J. J. Kim, *Adv. Mater.* **2016**, *28*, 2526.
[26] D. Zhou, G. S. M. Tong, G. Cheng, Y. K. Tang, W. Liu, D. Ma, L. Du, J. R. Chen, C.-M. Che, *Adv. Mater.* **2022**, *34*, 2206598.
[27] Y. Zhang, J. Wei, L. Wang, T. Huang, G. Meng, X. Wang, X. Zeng, M. Du, T. Fan, C. Yin, D. Zhang, L. Duan, *Adv. Mater.* **2023**, *35*, 2209396.
[28] J. G. Yang, X. Feng, N. Li, J. Li, X. F. Song, M. D. Li, G. Cui, J. Zhang, C. Jiang, C. Yang, K. Li, *Sci. Adv.* **2023**, *9*, eadh0198.
[29] R. M. Ciarnáin, H. W. Mo, K. Nagayoshi, H. Fujimoto, K. Harada, R. Gehlhaar, T. H. Ke, P. Heremans, C. Adachi, *Adv. Mater.* **2022**, *34*, 2201409.
[30] M. Shi, Y. He, Y. Sun, D. Fang, J. Miao, M. U. Ali, T. Wang, Y. Wang, T. Zhang, H. Meng, *Org. Electron.* **2020**, *84*, 105793.
[31] G. Li, L. Ameri, T. Fleetham, Z. Q. Zhu, J. Li, *Appl. Phys. Lett.* **2020**, *117*, 253301.
[32] Q. Wang, J. Ding, D. Ma, Y. Cheng, L. Wang, X. Jing, F. Wang, *Adv. Funct. Mater.* **2009**, *19*, 84.